INORGANIC CHEMISTRY FRONTIERS

RESEARCH ARTICLE

View Article Online
View Journal | View Issue

Cite this: *Inorg. Chem. Front.*, 2018, **5**, 1844

Efficient Co@CoP$_x$ core–shell nanochains catalyst for the oxygen evolution reaction†

Xiaotao Yuan,‡[a] Zhe Zhang,‡[a] Zichao Liu,[a] Xin Wang,[a] Chenlong Dong,[a] Muhammad Sohail Riaz[a] and Fuqiang Huang *[a,b]

Received 7th May 2018,
Accepted 29th May 2018

DOI: 10.1039/c8qi00428e

rsc.li/frontiers-inorganic

Co@CoP$_x$ core–shell nanochains were prepared *via* a direct-current arc-discharge method and subsequent phosphorization at 350 °C. The nanochains comprise nanospheres connected to each other with a length of several micrometers. The amount of CoP$_x$ can be easily changed by varying the phosphorization time. In the Co@CoP$_x$ core–shell structure, Co serves as a conductive channel, which improves the reaction kinetics of the oxygen evolution process on CoP$_x$. Co metal can also inject electrons into CoP$_x$, thus changing the work function of CoP$_x$ and improving its oxygen evolution efficiency. Based on the optimized structure, the Co@CoP$_x$ nanochains catalyst exhibits excellent oxygen evolution performance. Co@CoP$_x$ achieves an overpotential of 310 mV at a current density of 10 mA cm^{-2}, which is lower than that of CoP$_x$ (418 mV), Co (408 mV), and RuO$_2$ (317 mV). Furthermore, Co@CoP$_x$ exhibits good durability during the long-term electrochemical test.

Introduction

Electrochemical water splitting has drawn significant attention since it is an efficient way to obtain clean hydrogen fuel.[1–3] In electrochemical processes, overpotential is required to drive the sluggish oxygen evolution reaction (OER), which leads to significant energy loss.[4–7] Electrocatalysts with high activity and durability are anticipated to accelerate the oxygen evolution process. To date, RuO$_2$ and IrO$_2$ have been proven as the best catalysts for the OER; however, their high cost and elemental scarcity limit their use in commercial applications.[8–10]

Over the past decade, several abundant 3d transition metal-derived materials have shown promising applications in OER.[11–18] Cobalt-based materials, particularly cobalt phosphides, have been widely studied because of their low-cost and noble metal-like catalytic performance.[19–23] However, cobalt phosphides alone show limited OER catalytic activity because of their relatively low specific area and charge transfer efficiency. The preparation of carbon-supported materials is a strategy generally used to improve the catalytic performance of cobalt phosphides.[24–27] However, the synthesis of carbon materials is sometimes complicated. Coupling with metals can also improve the catalytic activity of the OER catalysts, as presented in our previous studies.[28–31] Conductive metals can accelerate the electron exchange process between the catalyst and electrolyte, thus improving the kinetics of the reaction. Metals can also inject electrons into the catalyst, thus changing its work function and improving the efficiency of OER. Preparing nanomaterials with one-dimensional structure is also an effective way to enhance the activity of OER catalysts since one-dimensional materials possess high specific surface areas and charge transfer efficiency.[32–34]

Herein, one-dimensional Co@CoP$_x$ core–shell nanochains were prepared *via* an arc-discharge method and subsequent phosphorization. The nanochains consist of uniform nanospheres with diameter of 30–50 nm. The length of the nanochains can extend to several micrometers. The amount of CoP$_x$ in Co@CoP$_x$ can be controlled by varying the phosphorization time. The Co@CoP$_x$ nanochains catalyst exhibits excellent catalytic activity for OER. The optimal sample achieves an overpotential of 310 mV at a current density of 10 mA cm^{-2}, which is superior to that of Co nanochains (408 mV), CoP$_x$ (418 mV), and RuO$_2$ (317 mV). Co@CoP$_x$ also exhibits good durability during the long-term test.

Experimental

Synthesis

The chemicals used in this study were of analytical reagent grade and used without further purification.

---

[a] *State Key Laboratory of Rare Earth Materials Chemistry and Applications, College of Chemistry and Molecular Engineering, Peking University, Beijing 100871, P.R. China*
[b] *State Key Laboratory of High Performance Ceramics and Superfine Microstructures. Shanghai Institute of Ceramics, Chinese Academy of Sciences, 1295 Dingxi Road, Shanghai 200050, P.R. China. E-mail: huangfq@pku.edu.cn*

† Electronic supplementary information (ESI) available: XRD pattern, TEM images of Co@CoP$_x$ nanochains, electrocatalytic properties of Co@CoP$_x$ nanochains. See DOI: 10.1039/c8qi00428e

‡ These authors contributed equally to this work.

Synthesis of Co nanochains

Co nanochains were synthesized *via* a direct current arc-discharge method, which was applied in our previous research studies.[31,32,35] The anode was a cobalt rod with diameter of 8 mm and the cathode was a pure graphite rod. The two electrodes were installed horizontally. The chamber was first evacuated to 3 Pa, and then filled with a gas mixture of He and H_2 to 0.08 MPa (pressure ratio, $He:H_2 = 2:1$). The reaction was carried out at 40 A, and the two electrodes were kept 2 mm away from each other by controlling the cathode.

Synthesis of Co@CoP$_x$ nanochains

Initially, 8 mg Co nanochains and 28.8 mg $NaH_2PO_2{\cdot}H_2O$ were placed separately in an evacuated quartz tube. The reaction was carried out at 350 °C for 15 min, 0.5 h, 1 h, 1.5 h and 2 h to obtain a series of Co@CoP$_x$ core–shell nanochains.

Synthesis of CoP$_x$

CoP$_x$ was synthesized the same way as Co@CoP$_x$, except the amount of $NaH_2PO_2{\cdot}H_2O$ was increased to 57.6 mg and the reaction time was extended to 12 h.

Characterization

Transmission electron microscope images (TEM) were acquired using a JEM-2100 at an accelerating voltage of 200 kV. Scanning electron microscope (SEM) images were acquired on a Hitachi S-4800 working at 10 kV. X-ray diffraction (XRD) was carried out on a Bruker D2 diffractometer using Cu K_α radiation (λ = 1.5418 Å). X-ray photoelectron spectroscopy (XPS) was carried out on an Axis Ultra Photoelectron Spectrometer (Kratos Analytical Ltd) using a monochromatized Al K_α anode (225 W, 15 mA, and 15 kV). The C 1s peak with binding energy of 284.8 eV was used for calibration.

Electrochemical measurement

The catalyst ink was prepared by dispersing 5 mg sample in 1 mL 0.5% Nafion solution under ultrasonic treatment. Then, 10 μL catalyst ink was casted onto a glassy carbon electrode with diameter of 5 mm The tests were performed on a CHI660E electrochemical workstation using a three-electrode system in 0.1 M KOH. The catalyst-modified electrode was used as the working electrode and Pt wire and Hg/HgO (1 M NaOH) were used as the counter and reference electrodes, respectively.

Cyclic voltammetry (CV) was carried out at a scan rate of 50 mV s^{-1}. Linear sweep voltammetry (LSV) data was collected at a scan rate of 5 mV s^{-1}. Both CV and LSV were performed in the range of 0 V to 1.0 V. Electrochemical impedance spectroscopy (EIS) was carried in the frequency ranging from 0.01 Hz to 100 kHz. Chronopotentiometry was conducted to evaluate the stability of the catalysts, and the current density was fixed at 10 mA cm^{-2}.

The electrochemical active surface area (ECSA) of the catalysts was acquired from a CV test in the region where no redox reaction occurs (0.05–0.1 V *vs.* Hg/HgO).[36,37] The ECSA is linearly proportional to the double-layer capacitance (C_{dl}), which can be calculated from the CV data.

Since Hg/HgO was used as the reference electrode, the data was calibrated to the RHE referring to the literature.[38] CV was performed in hydrogen saturated 0.1 M KOH at a scan rate of 1 mV s^{-1}. Platinum wire was used as the working and counter electrodes and Hg/HgO was used as the reference electrode. The average of the two potentials at zero current, which was determined to be 0.866 V, was used to calibrate the data:

$$E\ (vs.\ \mathrm{RHE}) = E\ (vs.\ \mathrm{Hg/HgO}) + 0.866$$

Results and discussion

The Co@CoP$_x$ core–shell nanochains were prepared *via* the phosphorization of arc-discharge derived Co nanochains (Fig. 1a). The Co nanochains and $NaH_2PO_2{\cdot}H_2O$ were placed separately in a quartz tube and the experiment was carried out at 350 °C. Fig. 1b shows the XRD patterns of Co@CoP$_x$ and Co nanochains (prepared under 1 h). The XRD pattern of the Co nanochains show diffraction peaks at 44.2°, 51.5° and 75.8°, which are indexed to the (111), (200) and (220) planes of Co with a face-centered cubic structure, respectively (JCPDS Card no. 15-0806). After phosphorization, new diffraction peaks appeared at 40.7°, 43.3° and 52.0°, which are assigned to the (121), (211) and (002) planes of Co_2P, respectively (JCPDS Card no. 32-0306). The small peaks at 31.6° and 48.1° can be assigned to CoP (JCPDS Card no. 29-0497).

SEM and TEM were used to study the detailed morphology of the samples. Co@CoP$_x$ exhibits a nanochain structure (Fig. 2a), which is similar to Co (Fig. S1†), indicating the retention of the structural integrity after phosphorization. The Co@CoP$_x$ nanochains exhibit a diameter of 50–60 nm and length of up to several micrometers. The TEM image (Fig. 2c) also indicates that the Co@CoP$_x$ nanochains possess a core–shell structure with shell thickness of about 10 nm. The shell of Co@CoP$_x$ does not show distinct lattice fringes because of the poor crystallinity of CoP$_x$.

Co@CoP$_x$ nanochains with phosphorization time of 15 min, 0.5 h, 1.5 h and 2 h were also prepared. The diffraction

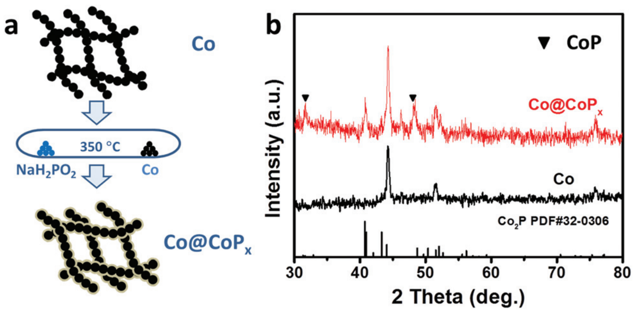

Fig. 1 (a) Schematic illustration of the synthesis of the Co@CoP$_x$ nanochains. (b) XRD patterns of Co and Co@CoP$_x$ nanochains (prepared under 1 h).

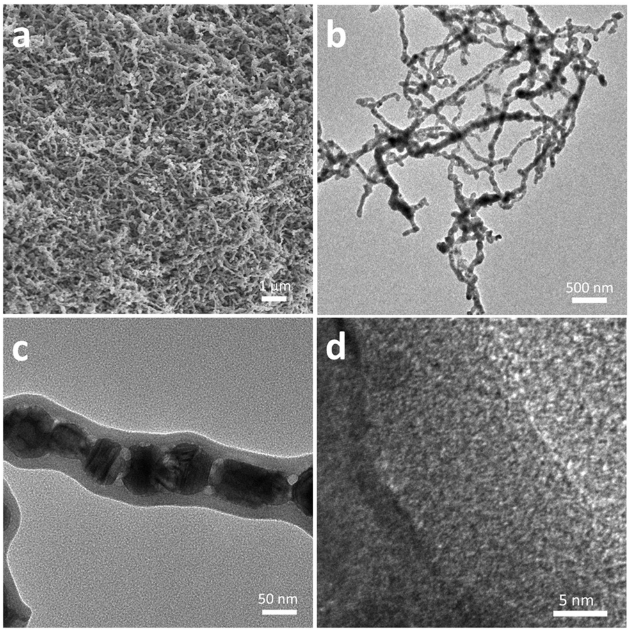

Fig. 2 (a) SEM image of the Co@CoP$_x$ nanochains (prepared under 1 h). (b–c) TEM and (d) HRTEM images of Co@CoP$_x$ nanochains (prepared under 1 h).

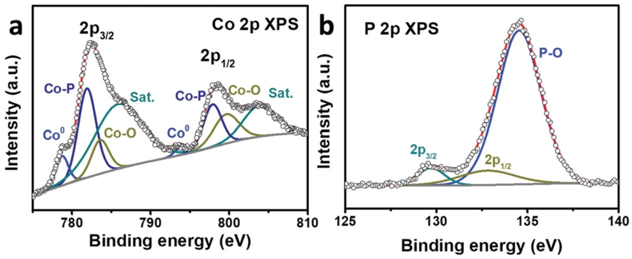

Fig. 3 (a) Co 2p and (b) P 2p high resolution XPS spectra of Co@CoP$_x$.

peak intensity and shell thickness of CoP$_x$ increase as the phosphorization time increased from 15 min to 2 h (Fig. S2†). The perfect core–shell nanochains were acquired at preparation times ranging from 15 min to 1 h (Fig. S3 and S4†). On extending the phosphorization time, some pores appeared, and the connection between the Co nanospheres was severed because of the consumption of Co, which may influence the conductivity of the nanochains and their application in electrocatalysis.

XPS was performed to analyze the composition and valence state of Co@CoP$_x$. The Co 2p spectrum can be deconvoluted into three spin–orbit doublets and two shakeup satellites (denoted as Sat.). The peaks located at 778.7 eV and 793.8 eV are assigned to the $2p_{3/2}$ and $2p_{1/2}$ states of Co^0, respectively. The doublets located at 781.9 and 797.8 eV can be attributed to the $2p_{3/2}$ and $2p_{1/2}$ states of Co bonded to P, while the doublets appearing at 783.55 and 799.6 eV can be ascribed to the $2p_{3/2}$ and $2p_{1/2}$ states of Co bonded to O, respectively.[39–42] The satellite peaks appear at 786.0 and 803.7 eV. Fig. 3b shows the P 2p XPS spectrum, which can be deconvoluted into three peaks. The peaks at 129.6 and 132.7 eV can be ascribed to the $2p_{3/2}$ and $2p_{1/2}$ core levels of P in CoP$_x$, respectively. The peak at 134.55 eV can be assigned to the oxidized P since the catalyst was exposed to air.

The OER catalytic performance of the Co@CoP$_x$ nanochains catalyst was studied using a three-electrode system in 0.1 M KOH, and the iR-corrected polarization curves were recorded. The CV curve of Co@CoP$_x$ displays distinct redox peaks before oxygen evolution (Fig. S6a†). The first redox couple (O_I/R_I) can be assigned to Co^{3+}/Co^{2+}, and the second redox couple (O_{II}/R_{II}) can be assigned to Co^{4+}/Co^{3+}. For comparison, the performances of CoP$_x$, Co and RuO$_2$ were also acquired in the same way. As shown in Fig. 4a, the Co@CoP$_x$ nanochains show superior performance to the Co nanochains and CoP$_x$ with higher current density and lower onset potential. When the current increases to 10 mA cm^{-2}, the Co@CoP$_x$ nanochains present an overpotential of 312 mV, which is much better than that of Co (408 mV), CoP$_x$ (310 mV) and also slightly superior to that of the RuO$_2$ catalyst (317 mV). The Co@CoP$_x$ nanochains exhibit a Tafel slope of 81.7 mV dec^{-1}, which is lower than that of Co (120 mV dec^{-1}) and CoP$_x$ (87.0 mV dec^{-1}), indicating its high OER kinetics. Since the catalytic process involves a valence state change in Co, the intense redox peak of Co@CoP$_x$ at 1.2 V also indicates that Co@CoP$_x$ has more catalytic sites than Co and CoP$_x$. The excellent OER performance of the Co@CoP$_x$ nanochains can be attributed to the synergistic effect between Co and CoP$_x$. CoP$_x$ is the catalytically active phase for OER, while the Co nanochains act as an electrical conductive channel, which promotes efficient electron exchange between the surface CoP$_x$ and the electrolyte. In addition to the synergistic effect, the electron injection process between Co and CoP$_x$ may also improve the OER performance of CoP$_x$ (Fig. 4c and d). The Fermi level of Co is higher than

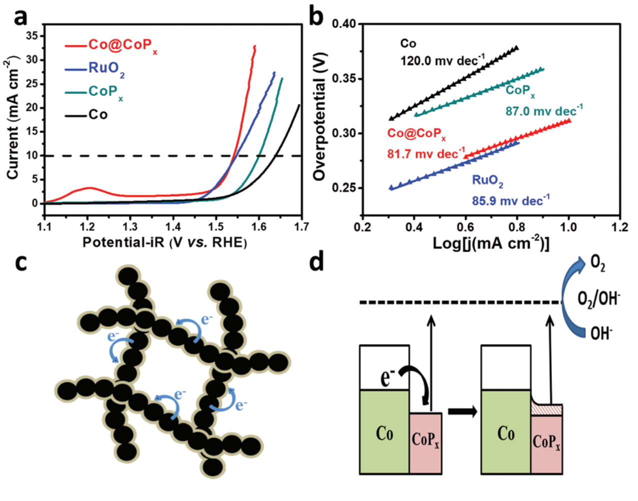

Fig. 4 (a) Polarization curves and (b) Tafel plots of Co, CoP$_x$, Co@CoP$_x$ and RuO$_2$. (c), (d) schematic illustration of the electron injection process between Co and CoP$_x$.

that of CoP_x; thus, Co can inject electrons into CoP_x and build up an internal electric field in their interface until they achieve the same Fermi level. This process manipulates the work function of CoP_x and reduces the overpotential needed to drive OER. The electron injection-promoted oxygen evolution process has been proven in our previous studies on metal–oxide and metal–sulfide heterostructures.[28,29] DFT calculations have proven that coupling with metals can change the adsorption energy of the reaction intermediates on oxides or sulfides, and thus change the rate determining step of the oxygen evolution process.[28,29]

To estimate the exposure of ion-accessible sites, the electrochemically active surface area (ECSA) was measured. The ECSA is linearly proportional to the electrochemical double layer capacitance (C_{dl}), which can be calculated from the cyclic voltammograms recorded in the region where no redox reaction occurs.[36,37] The CV curves of Co@CoP_x are presented in Fig. 5a and the CV curves of Co and CoP_x are presented in Fig. S6.† C_{dl} was acquired by plotting j (j_a–j_c) at 0.94 V (*vs.* RHE) against the scan rate, the slope of which is twice the C_{dl}. The result indicates that Co@CoP_x has much larger ECSA than CoP_x. CoP_x in Co@CoP_x is supported by Co nanochains, which can prevent CoP_x from aggregation during the reaction. A high ECSA means more catalytic active sites, which also contribute to the excellent OER performance of Co@CoP_x.

The effect of the CoP_x shell thickness on the OER activity of Co@CoP_x was also studied. The polarization curves of Co@CoP_x prepared with different phosphorization times are shown in Fig. 5c. CoP_x is the catalytically active phase in Co@CoP_x; thus, the OER performance initially improved with an increase in the amount of CoP_x and the sample prepared for 1 h shows the best catalytic activity. When the reaction time was further extended, the thickness of CoP_x increased and the interaction between Co and CoP_x decayed rapidly. The sample with long phosphorization time also show some pores in the Co nanochains (Fig. S4†). The electron transfer path was blocked by these pores, which reduced the electrical conductivity of the Co@CoP_x nanochains. Consequently, the catalytic performance of the samples prepared with longer reaction time decreased. The sample prepared for 1 h has the optimal structure and exhibits the best OER performance. Apart from its high catalytic activity, the Co@CoP_x composite also shows excellent durability for the OER. Fig. 5d shows the long-term chronopotentiometry test of Co@CoP_x and RuO_2. The performance of Co@CoP_x shows only a slight decay, while the overpotential of RuO_2 increased significantly since the surface RuO_2 is easily oxidized into water soluble RuO_4^{2-}.[43,44] The polarization curves and SEM image of Co@CoP_x after the stability test also indicate that the morphology of the sample changes only slightly during the oxygen evolution process (Fig. S8 and S9†).

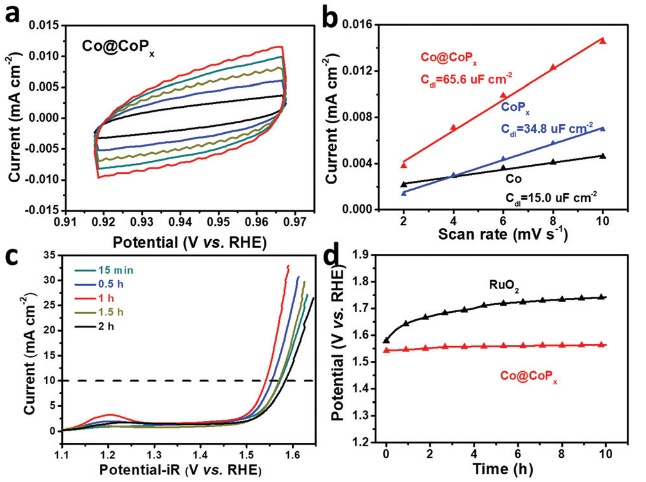

Fig. 5 (a) Cyclic voltammetry curves of Co@CoP_x in the region where no redox reaction occurs; the scan rates are 10, 8, 6, 4, and 2 mV s^{-1}. (b) Current density as a function of the scan rate for the Co nanochains, CoP_x and Co@CoP_x nanochains. (c) Polarization curves of the samples prepared under different phosphorization times. (d) Chronopotentiometry curves of Co@CoP_x and RuO_2.

Conclusions

In summary, Co@CoP_x core–shell nanochains were synthesized *via* an arc-discharge method and subsequent phosphorization process. The thickness of the CoP_x shell can be altered by controlling the phosphorization time. The sample prepared under 1 h exhibits optimal OER performance with an overpotential of 310 mV at the current density of 10 mA cm^{-2}, which is better than that of CoP_x (370 mV), Co (408 mV), and RuO_2 (317 mV). The high catalytic activity of Co@CoP_x can be attributed to the synergistic effect between Co and CoP_x. The highly conductive Co nanochains improve the kinetics of the OER on CoP_x, and the electron injection process from Co to CoP_x reduces the overpotential of OER. Apart from its high OER catalytic performance, the Co@CoP_x nanochains also exhibited good durability during the long-term test.

Conflicts of interest

There are no conflicts to declare.

Acknowledgements

This study was financially supported by National key R&D Program of China (Grant 2016YFB0901600), Science and Technology Commission of Shanghai (Grant 16JC1401700), the Key Research Program of Chinese Academy of Sciences (Grants No. QYZDJ-SSW-JSC013 and KGZD-EW-T06).

Notes and references

1 N. S. Lewis and D. G. Nocera, *Proc. Natl. Acad. Sci. U. S. A.*, 2006, **103**, 15729–15735.

2 M. Gao, W. Sheng, Z. Zhuang, Q. Fang, S. Gu, J. Jiang and Y. Yan, *J. Am. Chem. Soc.*, 2014, **136**, 7077–7084.

3 Z.-L. Wang, D. Xu, J.-J. Xu and X.-B. Zhang, *Chem. Soc. Rev.*, 2014, **43**, 7746–7786.
4 J. Suntivich, K. J. May, H. A. Gasteiger, J. B. Goodenough and Y. Shao-Horn, *Science*, 2011, **334**, 1383–1385.
5 H. Dau, C. Limberg, T. Reier, M. Risch, S. Roggan and P. Strasser, *ChemCatChem*, 2010, **2**, 724–761.
6 S. W. Lee, C. Carlton, M. Risch, Y. Surendranath, S. Chen, S. Furutsuki, A. Yamada, D. G. Nocera and Y. Shao-Horn, *J. Am. Chem. Soc.*, 2012, **134**, 16959–16962.
7 J. Wang, H. x. Zhong, Y. l. Qin and X. b. Zhang, *Angew. Chem., Int. Ed.*, 2013, **52**, 5248–5253.
8 F. Cheng and J. Chen, *Chem. Soc. Rev.*, 2012, **41**, 2172–2192.
9 C. C. L. McCrory, S. Jung, J. C. Peters and T. F. Jaramillo, *J. Am. Chem. Soc.*, 2013, **135**, 16977–16987.
10 Z. Chen, D. Cummins, B. N. Reinecke, E. Clark, M. K. Sunkara and T. F. Jaramillo, *Nano Lett.*, 2011, **11**, 4168–4175.
11 M. R. Gao, Y. F. Xu, J. Jiang, Y. R. Zheng and S. H. Yu, *J. Am. Chem. Soc.*, 2012, **134**, 2930–2933.
12 X.-Y. Yu, Y. Feng, B. Guan, X. W. Lou and U. Paik, *Energy Environ. Sci.*, 2016, **9**, 1246–1250.
13 A. Grimaud, K. J. May, C. E. Carlton, Y. L. Lee, M. Risch, W. T. Hong, J. Zhou and Y. Shao-Horn, *Nat. Commun.*, 2013, **4**, 2439.
14 L. Han, S. Dong and E. Wang, *Adv. Mater.*, 2016, **28**, 9266–9291.
15 J. Wang, W. Cui, Q. Liu, Z. Xing, A. M. Asiri and X. Sun, *Adv. Mater.*, 2016, **28**, 215–230.
16 B. M. Hunter, H. B. Gray and A. M. Muller, *Chem. Rev.*, 2016, **116**, 14120–14136.
17 N.-T. Suen, S.-F. Hung, Q. Quan, N. Zhang, Y.-J. Xu and H. M. Chen, *Chem. Soc. Rev.*, 2017, **46**, 337–365.
18 I. Roger, M. A. Shipman and M. D. Symes, *Nat. Rev. Chem.*, 2017, 1.
19 S. Anantharaj, S. R. Ede, K. Sakthikumar, K. Karthick, S. Mishra and S. Kundu, *ACS Catal.*, 2016, **6**, 8069–8097.
20 J. Ryu, N. Jung, J. H. Jang, H.-J. Kim and S. J. Yoo, *ACS Catal.*, 2015, **5**, 4066–4074.
21 Y.-P. Zhu, Y.-P. Liu, T.-Z. Ren and Z.-Y. Yuan, *Adv. Funct. Mater.*, 2015, **25**, 7337–7347.
22 L. Jiao, Y.-X. Zhou and H.-L. Jiang, *Chem. Sci.*, 2016, **7**, 1690–1695.
23 H. Yang, Y. Zhang, F. Hu and Q. Wang, *Nano Lett.*, 2015, **15**, 7616–7620.
24 D. Das and K. K. Nanda, *Nano Energy*, 2016, **30**, 303–311.
25 Z. H. Xue, H. Su, Q. Y. Yu, B. Zhang, H. H. Wang, X. H. Li and J. S. Chen, *Adv. Energy Mater.*, 2017, **7**, 7.
26 X. B. Yu, S. Zhang, C. Y. Li, C. L. Zhu, Y. J. Chen, P. Gao, L. H. Qi and X. T. Zhang, *Nanoscale*, 2016, **8**, 10902–10907.
27 P. Wang, F. Song, R. Amal, Y. H. Ng and X. L. Hu, *ChemSusChem*, 2016, **9**, 472–477.
28 X. Yuan, J. Yin, Z. Liu, X. Wang, C. Dong, W. Dong, M. S. Riaz, Z. Zhang, M. Chen and F. Huang, *ACS Appl. Mater. Interfaces*, 2018, **10**, 11565–11571.
29 X. Wang, X. Liu, C.-J. Tong, X. Yuan, W. Dong, T. Lin, L.-M. Liu and F. Huang, *J. Mater. Chem. A*, 2016, **4**, 7762–7771.
30 X. Yuan, M. S. Riaz, X. Wang, C. Dong, Z. Zhang and F. Huang, *Chem. – Eur. J.*, 2018, **24**, 3707–3711.
31 X. Yuan, H. Ge, X. Wang, C. Dong, W. Dong, M. S. Riaz, Z. Xu, J. Zhang and F. Huang, *ACS Energy Lett.*, 2017, **2**, 1208–1213.
32 Z. Xiong and X. S. Zhao, *J. Am. Chem. Soc.*, 2012, **134**, 5754–5757.
33 C. Sun, H. Li and L. Chen, *Energy Environ. Sci.*, 2012, **5**, 8475.
34 J. Tian, Y. Sang, Z. Zhao, W. Zhou, D. Wang, X. Kang, H. Liu, J. Wang, S. Chen and H. Cai, *Small*, 2013, **9**, 3864–3872.
35 X. Yuan, H. Ge, X. Liu, X. Wang, W. Chen, W. Dong and F. Huang, *J. Alloys Compd.*, 2016, **688**(Part A), 613–618.
36 J. Bao, X. Zhang, B. Fan, J. Zhang, M. Zhou, W. Yang, X. Hu, H. Wang, B. Pan and Y. Xie, *Angew. Chem., Int. Ed.*, 2015, **54**, 7399–7404.
37 J. Xie, X. Zhang, H. Zhang, J. Zhang, S. Li, R. Wang, B. Pan and Y. Xie, *Adv. Mater.*, 2017, **29**, 1604765.
38 Y. Liang, Y. Li, H. Wang, J. Zhou, J. Wang, T. Regier and H. Dai, *Nat. Mater.*, 2011, **10**, 780–786.
39 Y. Bai, H. Zhang, Y. Feng, L. Fang and Y. Wang, *J. Mater. Chem. A*, 2016, **4**, 9072–9079.
40 Y. Pan, Y. Lin, Y. Liu and C. Liu, *Catal. Sci. Technol.*, 2016, **6**, 1611–1615.
41 L. Ai, Z. Niu and J. Jiang, *Electrochim. Acta*, 2017, **242**, 355–363.
42 T. Liu, K. Wang, G. Du, A. M. Asiri and X. Sun, *J. Mater. Chem. A*, 2016, **4**, 13053–13057.
43 E. J. M. Osullivan and J. R. White, *J. Electrochem. Soc.*, 1989, **136**, 2576–2583.
44 S. Zhuiykov, *Proc. Int. Symp. Olfaction Electron. Noses*, 2009, **1137**, 34–37.